

Chiral Symmetry Breaking for Deterministic Switching of Perpendicular Magnetization by Spin–Orbit Torque

Hao Wu,* John Nance, Seyed Armin Razavi, David Lujan, Bingqian Dai, Yuxiang Liu, Haoran He, Baoshan Cui, Di Wu, Kin Wong, Kemal Sobotkiewich, Xiaoqin Li, Gregory P. Carman, and Kang L. Wang*



Cite This: *Nano Lett.* 2021, 21, 515–521



Read Online

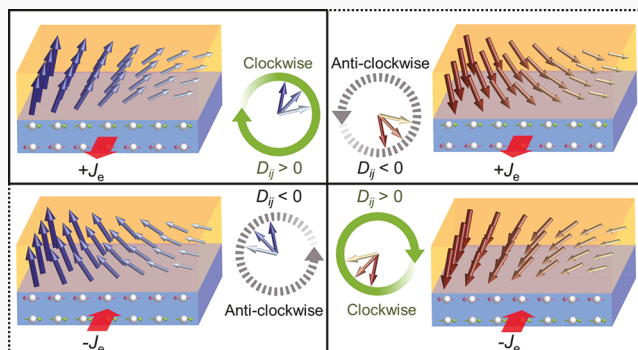
ACCESS |

Metrics & More

Article Recommendations

Supporting Information

ABSTRACT: Symmetry breaking is a characteristic to determine which branch of a bifurcation system follows upon crossing a critical point. Specifically, in spin–orbit torque (SOT) devices, a fundamental question arises: how can the symmetry of the perpendicular magnetic moment be broken by the in-plane spin polarization? Here, we show that the chiral symmetry breaking by the antisymmetric Dzyaloshinskii–Moriya interaction (DMI) can induce the deterministic SOT switching of the perpendicular magnetization. By introducing a gradient of saturation magnetization or magnetic anisotropy, the dynamic noncollinear spin textures are formed under the current-driven SOT, and thus, the chiral symmetry of these dynamic spin textures is broken by the DMI, resulting in the deterministic magnetization switching. We introduce a strategy to induce an out-of-plane (z) gradient of magnetic properties as a practical solution for the wafer-scale manufacture of SOT devices.



We introduce a strategy to induce an out-of-plane (z) gradient of magnetic properties as a practical solution for the wafer-scale manufacture of SOT devices.

KEYWORDS: chiral symmetry breaking, Dzyaloshinskii–Moriya interaction, spin–orbit torque, magnetic gradient

Symmetry is a fundamental characteristic of a system that is preserved under some transformations. Symmetry breaking often results in important phenomena in physics, such as quantized conductance and superconductivity.¹ In spintronics, the symmetry of the perpendicular magnetization is preserved under the current induced spin–orbit torque (SOT),^{2–4} and hence, the SOT switching is nondeterministic. SOT originates from a vertical spin current (J_s) injection from an adjacent layer or interface with strong spin–orbit coupling by an in-plane (electric) charge current (J_e), via the way of spin Hall effect⁵ or Rashba effect,⁶ and the spin polarization σ is along the in-plane direction according to $J_s \propto \sigma \times J_e$; therefore, for the magnetization with perpendicular magnetic anisotropy (PMA),^{7,8} the spins with in-plane polarization [damping-like torque $\tau_{\text{SOT}} \propto m \times (m \times \sigma)$] cannot break the symmetry between perpendicular magnetizations of $\pm M_z$, where m represents the unit vector of the magnetic moment, leading to the nondeterministic nature of SOT switching. In order to realize the deterministic SOT switching of the perpendicular magnetization, several methods have been developed to break the mirror symmetry, such as an external or internal in-plane magnetic field,^{9–13} tilted magnetic anisotropy,¹⁴ lateral structural asymmetry or spin current asymmetry,^{15–18} and competing spin currents.¹⁹

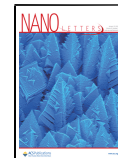
An antisymmetric exchange interaction, i.e., Dzyaloshinskii–Moriya interaction (DMI),^{20,21} presents in systems without inversion symmetry and stabilizes the noncollinear spin canting between neighboring magnetic moments. DMI induces the chiral spin textures such as magnetic skyrmions²² and the chiral magnetic coupling.^{23–25} The Hamiltonian of DMI can be written as $\hat{H}_{\text{DMI}} = \sum_{i,j} -D_{ij} \cdot (m_i \times m_j)$, where D_{ij} is the DMI tensor between m_i and m_j . As a consequence of the minimized DMI energy, DMI breaks the chiral symmetry of noncollinear spin textures and determines the spin canting direction of clockwise ($D_{ij} > 0$) or anticlockwise ($D_{ij} < 0$). In the Fert–Levy model,^{26–28} the interfacial DMI satisfies $D_{ij} = D_{ij}(r_i \times r_j)$, where D_{ij} is the interfacial DMI coefficient, as shown in Figure 1a.

Here, we report the chiral symmetry breaking by DMI for deterministic SOT switching of the perpendicular magnetiza-

Received: October 5, 2020

Revised: December 8, 2020

Published: December 18, 2020



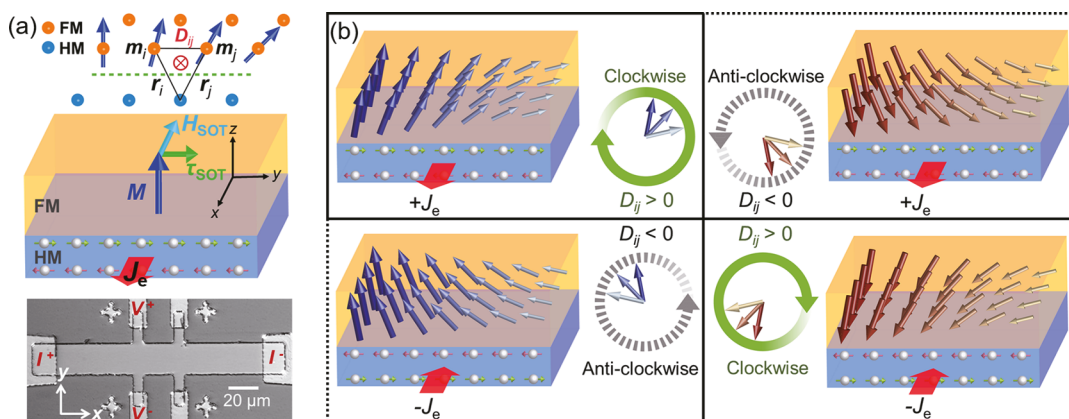


Figure 1. Concept of deterministic spin–orbit torque (SOT) switching by chiral symmetry breaking. (a) The spin current in the heavy metal (HM) generated by the spin Hall effect exerts a torque τ_{SOT} on the adjacent magnet (FM) with perpendicular magnetic anisotropy (PMA), which can be described by an effective field H_{SOT} , where J_e is the charge current. The schematic of the interfacial Dzyaloshinskii–Moriya interaction (DMI) ($D_{ij} > 0$), which stabilizes the clockwise chirality. The bottom figure shows the experiment set up in the Hall bar device. (b) Under the current-driven SOT, if there is a gradient of the total effective field ∇H_{eff} , the canting angle of magnetizations has a spatial nonuniform gradient distribution, which forms the dynamic noncollinear spin textures ($m_i \times m_j$), resulting in an additional dynamic DMI energy in the system. There are four possible states for different current and magnetization configurations, where the chiral symmetry is broken by the DMI ($D_{ij} > 0$ for clockwise or $D_{ij} < 0$ for anticlockwise), leading to the deterministic magnetization switching.

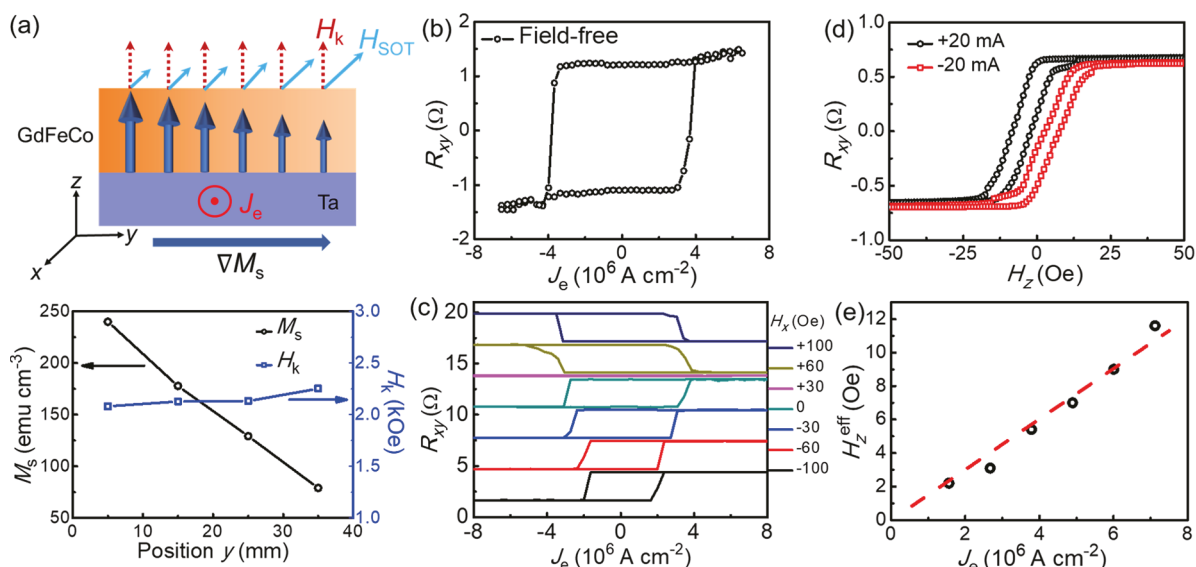


Figure 2. Chiral symmetry breaking determined SOT switching with an in-plane gradient of M_s ($\nabla_y M_s$). (a) The composition gradient along the y -direction in Ta/Gd_x(FeCo)_{1-x} leads to a saturation magnetization gradient $\nabla_y M_s$ (49 emu cm⁻³), where the magnetic anisotropy field, H_k , is almost constant. (b) Current-driven SOT switching without the external magnetic field. (c) SOT switching with a series of the in-plane magnetic field, H_x . (d) R_{xy} – H_z curves with ± 20 mA currents show the SOT-induced hysteresis loop shift. (e) Out-of-plane effective field H_z^{eff} of SOT as a function of J_e .

ization. By introducing a gradient of saturation magnetization (M_s) or magnetic anisotropy field (H_k), the dynamic noncollinear spin textures are formed under the current-driven SOT, where DMI breaks the chiral symmetry of these dynamic spin textures, resulting in the deterministic SOT switching. We experimentally demonstrate this concept in three representative cases: in-plane gradient of M_s in the Ta/Gd_x(FeCo)_{1-x} system; in-plane gradient of H_k in the Ta/CoFeB (wedge)/MgO system; out-of-plane gradient of M_s in the Ta/[Gd_x(FeCo)_{1-x}]₆ and Ta/CoFeB/CoFe/MgO systems. The last case of an out-of-plane M_s gradient can be applied in the wafer-scale manufacture. Different from previous works based on the gradient-induced additional spin-torque,^{15–18} in this work, we take the antisymmetric DMI into consideration and

use the resulting chiral symmetry breaking to determine the SOT switching.

Figure 1a shows the current-induced SOT in the heavy metal/ferromagnet system in a 20 $\mu\text{m} \times 130 \mu\text{m}$ Hall bar device. A 1 ms writing current pulse J_e is applied to provide the SOT first, followed by a 1 ms reading current pulse (1 mA) to detect the magnetization by the anomalous Hall resistance at 1-s later, where the effective field of SOT can be written as $H_{\text{SOT}} = H_{\text{SOT}} (\mathbf{m} \times \boldsymbol{\sigma})$. By considering the SOT and DMI contributions, the total effective field can be written as $H_{\text{eff}} = H_{\text{ex}} + H_{\text{DMI}} + H_{\text{SOT}} + H_k$, where $H_{\text{ex}} = H_{\text{ex}} \Delta \mathbf{m}$, $H_{\text{DMI}} = H_{\text{DMI}} [(\nabla \cdot \mathbf{m}) \hat{z} - \nabla m_z]$, and $H_k = H_k \hat{z}$ represent the effective fields of exchange interaction, DMI, and perpendicular magnetic anisotropy, respectively. Under the current-

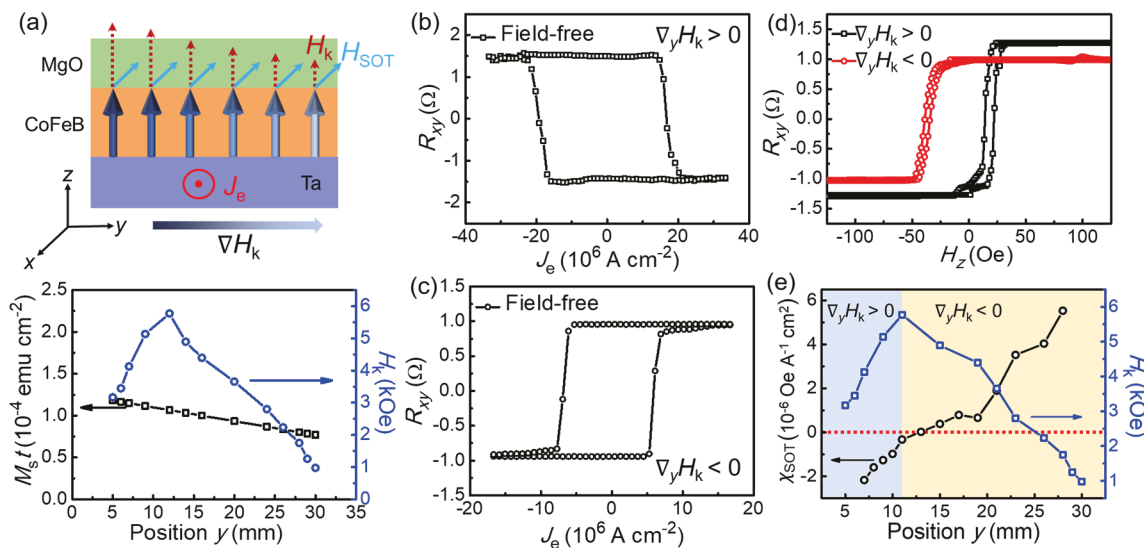


Figure 3. Chiral symmetry breaking determined SOT switching with an in-plane gradient of H_k ($\nabla_y H_k$). (a) In the Ta/CoFeB (wedge)/MgO system, the magnetic anisotropy field H_k from the interfacial PMA could be modulated by varying the thickness of CoFeB, resulting in a $\nabla_y H_k$ along the y -direction. (b, c) The field-free SOT switching in $\nabla_y H_k > 0$ and $\nabla_y H_k < 0$ cases, respectively, where the switching polarity is opposite in these two cases. (d) SOT-induced hysteresis loops are shifted to the opposite field directions in $\nabla_y H_k > 0$ and $\nabla_y H_k < 0$ cases under the same current (20 mA). (e) SOT-induced out-of-plane effective field χ_{SOT} as a function of device positions, where χ_{SOT} changes the sign from the $\nabla_y H_k > 0$ region to the $\nabla_y H_k < 0$ region.

driven SOT, if there is a spatial gradient of the total effective field H_{eff} i.e., ∇H_{eff} , the canting angle of magnetizations has a spatial nonuniform gradient distribution, and thus the dynamic noncollinear spin textures ($m_i \times m_j$) can be formed by SOT, resulting in an additional dynamic DMI energy ΔE_{DMI} in the system.

Figure 1b shows the four possible states for different current and magnetization configurations. For a positive DMI coefficient ($D_{ij} > 0$), such as in the Ta/Ferromagnet system,²⁹ the clockwise chirality of spin textures is preferred due to the minimized DMI energy. The chirality of the SOT-induced dynamic spin textures is illustrated in Figure 1b, where DMI breaks the chiral symmetry of these four possible states: for $D_{ij} > 0$ (or $D_{ij} < 0$), selects the clockwise (or anticlockwise) chirality of $(+J_e, +M_z)$ and $(-J_e, -M_z)$ states [or $(+J_e, -M_z)$ and $(-J_e, +M_z)$ states]. Once the current is removed, the spin texture will return to its stable magnetic anisotropy direction ($\pm z$); as a result, deterministic SOT switching is achieved.

In the heavy metal/ferrimagnet [Ta/Gd_x(FeCo)_{1-x}] system, M_s could be controlled by the composition of the ferrimagnet Gd_x(FeCo)_{1-x} due to the antiferromagnetically coupled Gd and FeCo spin sublattices.³⁰ By cosputtering the off-axis Gd and FeCo targets in the opposite directions with the same speed, a composition gradient is formed (x from 0.14 to 0.22), where the thickness of Gd_x(FeCo)_{1-x} film keeps uniform (Figure S3). As a result of this composition gradient, a saturation magnetization gradient $\nabla_y M_s$ (49 emu cm⁻⁴) is generated along the y -direction, at the same time the magnetic anisotropy field H_k has no obvious variation, as shown in Figure 2a, where M_s and H_k are measured in 5 mm × 5 mm pieces at different positions. According to the SOT effective field $H_{\text{SOT}} = \frac{\hbar e H_{\text{SH}}}{2|e| M_s t}$, $\nabla_y M_s$ induces a $\nabla_y H_{\text{SOT}}$ and thus the resulting gradient of the total effective field $\nabla_y H_{\text{eff}}$ therefore, the $\nabla_y H_{\text{eff}}$ -induced spatial nonuniform gradient distribution of the canting angle of magnetizations forms the dynamic spin textures under SOT, where \hbar is the reduced Planck constant, t

is the thickness of the magnetic layer, and e is the elementary charge. From Brillouin scattering (BLS) spectroscopy, we can obtain a positive D_{ij} of $15.2 \mu\text{J m}^{-2}$ in this system (Figure S2), which stabilizes the clockwise chirality. The clockwise chirality in this system is also verified by the asymmetric magnetic domain nucleation (Figure S4).³¹

Then, we perform the measurement of SOT switching in the Ta/Gd_x(FeCo)_{1-x} system with a saturation magnetization gradient $\nabla_y M_s$. For J_e along the x -axis, the $\nabla_y M_s$ -induced dynamic spin texture is formed in the $y-z$ plane along the y -direction, where DMI selects the clockwise chirality and determines the magnetization switching without an external magnetic field, with a switching current density $J_c = 4.0 \times 10^6 \text{ A cm}^{-2}$, as shown in Figure 2b. It is known that the chirality of spin textures could also be modified by the external magnetic field, and thus we perform the SOT switching by scanning the H_x , as shown in Figure 2c. The deterministic switching vanishes at $H_x = +30$ Oe, indicating an effective field $H_{\text{DMI}} = -30$ Oe of DMI, which is consistent with the estimated $H_{\text{DMI}} = -\frac{D}{\mu_0 M_s \delta_{\text{DW}}} = -26.4$ Oe from the BLS measurement,

where $\delta_{\text{DW}} = \pi \left(\frac{A}{K} \right)^{1/2}$ is the domain wall width, and A ($4 \times 10^{-12} \text{ J m}^{-1}$) and K ($2 \times 10^4 \text{ J m}^{-3}$) represent the exchange stiffness constant and the PMA energy, respectively.³² The opposite polarity of SOT switching at $\pm H_x$ above 60 Oe originates from the dominating contribution from the magnetic field (Figure 2c).

The current-induced hysteresis loop shift method is employed to extract the out-of-plane effective field H_z^{eff} of the field-free SOT for the Ta/Gd_x(FeCo)_{1-x} system, where the center fields (H_{zc}^+ and H_{zc}^-) of $R_{xy}-H_z$ curves under ± 20 mA are shifted to the opposite directions, as shown in Figure 2d. Figure 2e shows the $H_z^{\text{eff}} = -(H_{zc}^+ - H_{zc}^-)/2$ as a function of J_e , and the linear dependence shows the typical SOT characteristic.

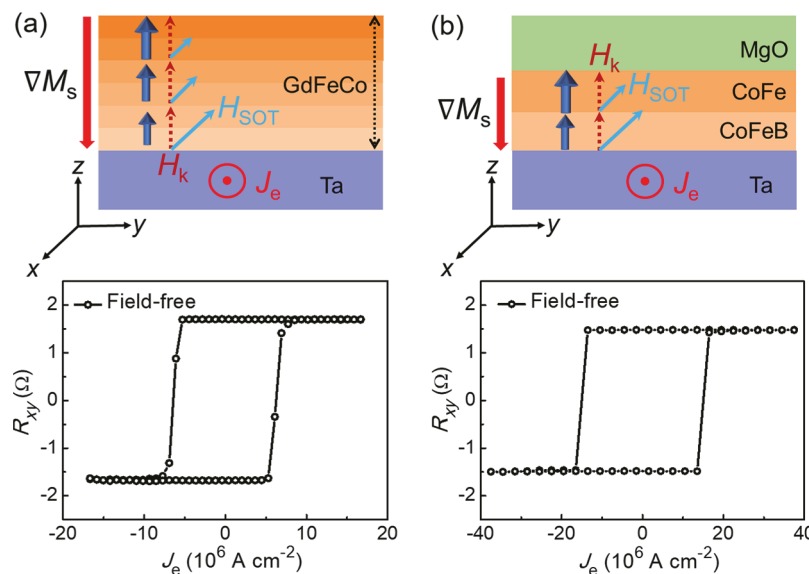


Figure 4. Chiral symmetry breaking determined SOT switching with an out-of-plane gradient of M_s ($\nabla_z M_s$). The chiral symmetry breaking determined SOT switching is robust in the ferrimagnet-based Ta/[$Gd_x(FeCo)_{1-x}$]₆ system with 6 magnetic layers with increasing M_s (a) and in the ferromagnet-based Ta/CoFeB/CoFe/MgO system with a magnetic bilayer (b), where the $\nabla_z M_s$ exists along the thickness (z) direction.

In fact, the chiral symmetry breaking determined SOT switching is independent of the ferrimagnetic properties. Next, we demonstrate the same mechanism for a ferromagnetic CoFeB layer in the Ta/CoFeB/MgO system, where the PMA comes from the CoFeB/MgO interface and thus can be controlled by the thickness of the CoFeB layer.³³ We design a wedged CoFeB layer with a thickness ranging from 1.24 to 0.8 nm, where the CoFeB thickness has a slight gradient along the y -direction. The H_k in devices at different positions (y) is measured by the saturation field of the R_{xy} - H_x curve. As shown in Figure 3a, H_k shows the maximum at $y = 12$ mm ($t_{CoFeB} = 1.1$ nm) due to the optimal Fe–O and Co–O bonds at the interface, where $\nabla_y H_k > 0$ in the range of $y < 12$ mm ($t_{CoFeB} > 1.1$ nm) and $\nabla_y H_k < 0$ in the range of $y > 12$ mm ($t_{CoFeB} < 1.1$ nm), due to the underoxidation and overoxidation induced PMA reduction, respectively.³⁴ The oxidation state in this system can be proved by the X-ray photoelectron spectroscopy (XPS) results in our previous work.³⁵ In this case, we neglect the slight gradient of the total magnetization ($M_s t_{CoFeB}$).

Then, we perform the SOT switching in the Ta/CoFeB (wedge)/MgO system (DMI coefficient: ³⁶ 54.0 $\mu\text{J m}^{-2}$). Under the current-driven SOT, according to $H_{\text{eff}} = H_{\text{ex}} + H_{\text{DMI}} + H_{\text{SOT}} + H_k$, $\nabla_y H_k$ contributes to a gradient of the total effective field $\nabla_y H_{\text{eff}}$ and thus the canting angle of magnetizations has a spatial nonuniform gradient distribution, which forms the dynamic spin textures. Similar to the $\nabla_y M_s$ case in Ta/ $Gd_x(FeCo)_{1-x}$, the deterministic magnetization switching happens due to the chiral symmetry breaking of the dynamic spin textures by DMI. It is worth noticing that in the devices with opposite $\nabla_y H_k$, i.e., $\nabla_y H_k > 0$ and $\nabla_y H_k < 0$, the gradient of the total effective field $\nabla_y H_{\text{eff}}$ changes the direction, and thus reverses the SOT-induced spin canting direction between neighboring magnetic moments from $\mathbf{m}_j \rightarrow \mathbf{m}_i$ to $\mathbf{m}_i \rightarrow \mathbf{m}_j$, i.e., reverses the chirality of SOT-induced dynamic spin textures ($\mathbf{m}_i \times \mathbf{m}_j$). The DMI selects the same chirality (clockwise) for $\nabla_y H_k > 0$ and $\nabla_y H_k < 0$ cases, resulting in the opposite polarity of the field-free SOT switching, as shown in Figure 3b,c. The polarity changes of the field-free SOT switching for $\nabla_y H_k > 0$ and $\nabla_y H_k < 0$ regions also indicate that the slightly structural

asymmetry of the wedged CoFeB layer is not the reason for deterministic switching because it is always along the same direction in all positions; otherwise, the switching polarity should be the same.^{15,18}

The current-induced hysteresis loop shift method is employed to analyze the relation between SOT-induced H_z^{eff} and $\nabla_y H_k$, as shown in Figure 3d,e, where the H_{zc}^+ of R_{xy} - H_z curves under the same current (+20 mA) are shifted to the opposite directions: $H_{zc}^+ = +18$ Oe for $\nabla_y H_k > 0$ and $H_{zc}^+ = -37$ Oe for $\nabla_y H_k < 0$, respectively, which is consistent with the reversed polarity of the field-free SOT switching in these two devices. We plot the $\chi_{\text{SOT}} = H_z^{\text{eff}}/J_e$ and $\nabla_y H_k$ as a function of position y , as shown in Figure 3e. The boundary between $\nabla_y H_k > 0$ region and $\nabla_y H_k < 0$ region is around $y = 11$ mm ($t_{CoFeB} = 1.08$ nm), where χ_{SOT} changes the sign just across this boundary, indicating the dominating contribution of $\nabla_y H_k$ on the field-free SOT.

The above methods of the lateral gradient lead to the variation of device properties across the wafer. In order to address this issue, we use the out-of-plane M_s gradient $\nabla_z M_s$ in the multilayer stack to achieve uniform magnetic properties laterally in the wafer scale, i.e., 6 sublayers (totally 4 nm) of $Gd_x(FeCo)_{1-x}$ with increasing M_s from 100 emu cm⁻³ to 200 emu cm⁻³ (x from 0.21 to 0.16), where the composition for each sublayer is characterized by the deposition speed of Gd and CoFe at different power. In this case, the SOT-induced dynamic spin textures are along the thickness direction (z); therefore, the interfacial DMI contribution in the heavy metal/ferrimagnet interface should vanish due to $\Delta E_{\text{DMI}} = \sum_{i,j} -D_{ij}(\mathbf{r}_i \times \mathbf{r}_j) \cdot (\mathbf{m}_i \times \mathbf{m}_j) = 0$. However, in the $Gd_x(FeCo)_{1-x}$ multilayer, the bulk (interlayer) DMI can still break the chiral symmetry and determine the SOT switching without an external field (Figure 4a), which may come from the slightly lateral crystal symmetry breaking as in previous works.^{24,25,37} The DMI energy is proportional to both the DMI coefficient D and the canted angle of neighboring magnetizations ($\mathbf{m}_i \times \mathbf{m}_j$), where the canted angle ($\mathbf{m}_i \times \mathbf{m}_j$) is proportional to the magnetization gradient ∇M_s , i.e., $\Delta E_{\text{DMI}} \propto D \nabla M_s$. Even for the relatively small bulk DMI ($D = 0.44$ μJ

m^{-2}), due to $\nabla_z M_s$ is dramatically enhanced along the thickness direction (2×10^8 emu cm^{-4}), ΔE_{DMI} can still determine the field-free SOT switching. The bulk (interlayer) DMI in multilayers has also been proved by the chiral interlayer exchange coupling phenomenon,^{24,25} and the spin textures along the thickness direction have also been demonstrated,^{38,39} which support our argument.

Furthermore, for the CoFeB(0.5 nm)/CoFe(0.5 nm) bilayer with a slight difference of M_s (955 and 1150 eum cm^{-3} for CoFeB and CoFe, respectively) in the Ta/CoFeB/CoFe/MgO structure, the chiral symmetry breaking determined SOT switching remains robust, as shown in Figure 4b. This structure can be directly integrated with the wafer-scale magnetic tunnel junction in today's magnetic memory technology.^{40,41}

In summary, by introducing a gradient of magnetic properties such as saturation magnetization and magnetic anisotropy, we demonstrate that the dynamic noncollinear spin textures could be formed in PMA materials under the current-driven SOT, and thus the chiral symmetry of the SOT-driven dynamic spin textures is broken by the intrinsic DMI (clockwise for $D_{ij} > 0$), resulting in the deterministic magnetization switching. The chiral symmetry breaking method by DMI is topologically protected; therefore, it is robust against defects and boundaries in nanodevices.

MATERIALS AND METHODS

The Ta/Gd_x(FeCo)_{1-x} and Ta/CoFeB (wedged)/MgO samples are grown by a magnetron sputtering method with a base pressure of 1×10^{-8} Torr. In situ 250 °C annealing is performed in the Ta/CoFeB (wedged)/MgO sample to increase the PMA. The Gd_x(FeCo)_{1-x} film is deposited by cosputtering the off-axis Gd and CoFe targets in the opposite side (along the y -axis) at the same speed (0.34 Å/s) without rotating the substrate; therefore, a composition gradient is formed along the y -direction, where the thickness keeps uniform. The power for Gd and CoFe targets is 20 and 95 W, respectively, and the Ar pressure for deposition is 3 mTorr. The wedged CoFeB layer is deposited by the off-axis sputtering of the CoFeB target without rotating the substrate (3 mTorr, 100 W), and the center thickness is 1.0 nm. The Ta/GdFeCo(6 layers) and Ta/CoFeB/CoFe/MgO samples (∇M_s along the thickness direction) are deposited by a similar method; however, the substrates keep rotating during the deposition of all layers so that the film properties are uniform in the wafer scale.

The films are patterned into Hall bar devices with a 20 μ m width by the standard photolithography method combined with a dry etching process, and the Cr (20 nm)/Au (100 nm) electrodes are fabricated for the contact of the Hall bar channel.

ASSOCIATED CONTENT

Supporting Information

The Supporting Information is available free of charge at <https://pubs.acs.org/doi/10.1021/acs.nanolett.0c03972>.

Micromagnetic simulation results; BLS measurements; methods for the composition gradient and the wedged thickness; asymmetric magnetic domain nucleation; anomalous Hall loops; angular dependence of field-free SOT switching; SOT switching under a series of in-plane fields; SOT switching with uniform magnetic properties; harmonic Hall measurement; method to

obtain H_k ; $M-H$ loops; Pt/Co (wedged)/MgO system; field-free SOT switching with opposite $\nabla_z M_s$; angular dependent magnetoresistance ([PDF](#))

AUTHOR INFORMATION

Corresponding Authors

Hao Wu – Department of Electrical and Computer Engineering, and Department of Physics and Astronomy, University of California, Los Angeles, California 90095, United States; orcid.org/0000-0001-8608-3035; Email: wuhaphysics@ucla.edu

Kang L. Wang – Department of Electrical and Computer Engineering, and Department of Physics and Astronomy, University of California, Los Angeles, California 90095, United States; orcid.org/0000-0003-0487-5464; Email: wang@ee.ucla.edu

Authors

John Nance – Department of Mechanical and Aerospace Engineering, University of California, Los Angeles, California 90095, United States

Seyed Armin Razavi – Department of Electrical and Computer Engineering, and Department of Physics and Astronomy, University of California, Los Angeles, California 90095, United States

David Lujan – Department of Physics, and Center for Complex Quantum Systems, The University of Texas at Austin, Texas 78712, United States

Bingqian Dai – Department of Electrical and Computer Engineering, and Department of Physics and Astronomy, University of California, Los Angeles, California 90095, United States

Yuxiang Liu – Department of Electrical and Computer Engineering, and Department of Physics and Astronomy, University of California, Los Angeles, California 90095, United States

Haoran He – Department of Electrical and Computer Engineering, and Department of Physics and Astronomy, University of California, Los Angeles, California 90095, United States

Baoshan Cui – Department of Electrical and Computer Engineering, and Department of Physics and Astronomy, University of California, Los Angeles, California 90095, United States

Di Wu – Department of Electrical and Computer Engineering, and Department of Physics and Astronomy, University of California, Los Angeles, California 90095, United States

Kin Wong – Department of Electrical and Computer Engineering, and Department of Physics and Astronomy, University of California, Los Angeles, California 90095, United States

Kemal Sobotkiewich – Department of Physics, and Center for Complex Quantum Systems, The University of Texas at Austin, Texas 78712, United States

Xiaoqin Li – Department of Physics, and Center for Complex Quantum Systems, The University of Texas at Austin, Texas 78712, United States

Gregory P. Carman – Department of Mechanical and Aerospace Engineering, University of California, Los Angeles, California 90095, United States

Complete contact information is available at:
<https://pubs.acs.org/10.1021/acs.nanolett.0c03972>

Author Contributions

H.W. and K.L.W. conceived and supervised the project. H.W. and S.A.R. grew materials. K.W. fabricated devices. H.W., B.D., and H.H. performed magnetic and MOKE measurements. H.W., S.A.R., and B.C. performed electrical transport measurements. J.N. and H.W. performed micromagnetic simulations. D.L. performed BLS measurements and analyzed the results together with K.S. and X.L. H.W., K.L.W., and S.A.R. analyzed the data. All authors contributed to discussions. H.W. and K.L.W. wrote the manuscript with input from all authors.

Notes

The authors declare no competing financial interest.

ACKNOWLEDGMENTS

This work is supported by the NSF Award Nos. 1935362, 1909416, and 1619027, the Nanosystems Engineering Research Center for Translational Applications of Nanoscale Multiferroic Systems (TANMS), the U.S. Army Research Office MURI program under Grants No. W911NF-16-1-0472, and the Spins and Heat in Nanoscale Electronic Systems (SHINES) Center funded by the US Department of Energy (DOE), under Award No. DE-SC0012670. D.L. and X.L. are funded by an NSF MRSEC under Cooperative Agreement No. DMR-1720595.

REFERENCES

- (1) Anderson, P. W. More is different. *Science* **1972**, *177*, 393.
- (2) Liu, L.; Pai, C.-F.; Li, Y.; Tseng, H. W.; Ralph, D. C.; Buhrman, R. A. Spin-Torque Switching with the Giant Spin Hall Effect of Tantalum. *Science* **2012**, *336*, 555.
- (3) Liu, L.; Lee, O. J.; Gudmundsen, T. J.; Ralph, D. C.; Buhrman, R. A. Current-Induced Switching of Perpendicularly Magnetized Magnetic Layers Using Spin Torque from the Spin Hall Effect. *Phys. Rev. Lett.* **2012**, *109*, 096602.
- (4) Miron, I. M.; Garello, K.; Gaudin, G.; Zermatten, P.-J.; Costache, M. V.; Auffret, S.; Bandiera, S.; Rodmacq, B.; Schuhl, A.; Gambardella, P. Perpendicular switching of a single ferromagnetic layer induced by in-plane current injection. *Nature* **2011**, *476*, 189.
- (5) Sinova, J.; Valenzuela, S. O.; Wunderlich, J.; Back, C. H.; Jungwirth, T. Spin Hall effects. *Rev. Mod. Phys.* **2015**, *87*, 1213.
- (6) Manchon, A.; Koo, H. C.; Nitta, J.; Frolov, S. M.; Duine, R. A. New perspectives for Rashba spin-orbit coupling. *Nat. Mater.* **2015**, *14*, 871.
- (7) Ikeda, S.; Miura, K.; Yamamoto, H.; Mizunuma, K.; Gan, H. D.; Endo, M.; Kanai, S.; Hayakawa, J.; Matsukura, F.; Ohno, H. A perpendicularly-anisotropy CoFeB–MgO magnetic tunnel junction. *Nat. Mater.* **2010**, *9*, 721.
- (8) Dieny, B.; Chshiev, M. Perpendicular magnetic anisotropy at transition metal/oxide interfaces and applications. *Rev. Mod. Phys.* **2017**, *89*, 025008.
- (9) Lau, Y.-C.; Betto, D.; Rode, K.; Coey, J. M. D.; Stamenov, P. Spin-orbit torque switching without an external field using interlayer exchange coupling. *Nat. Nanotechnol.* **2016**, *11*, 758.
- (10) Oh, Y.-W.; Chris Baek, S.-h.; Kim, Y. M.; Lee, H. Y.; Lee, K.-D.; Yang, C.-G.; Park, E.-S.; Lee, K.-S.; Kim, K.-W.; Go, G.; Jeong, J.-R.; Min, B.-C.; Lee, H.-W.; Lee, K.-J.; Park, B.-G. Field-free switching of perpendicular magnetization through spin-orbit torque in antiferromagnet/ferromagnet/oxide structures. *Nat. Nanotechnol.* **2016**, *11*, 878.
- (11) Fukami, S.; Zhang, C.; DuttaGupta, S.; Kurenkov, A.; Ohno, H. Magnetization switching by spin-orbit torque in an antiferromagnet–ferromagnet bilayer system. *Nat. Mater.* **2016**, *15*, 535.
- (12) Wang, X.; Wan, C.; Kong, W.; Zhang, X.; Xing, Y.; Fang, C.; Tao, B.; Yang, W.; Huang, L.; Wu, H.; Irfan, M.; Han, X. Field-Free Programmable Spin Logics via Chirality-Reversible Spin–Orbit Torque Switching. *Adv. Mater.* **2018**, *30*, 1801318.
- (13) Baek, S. C.; Amin, V. P.; Oh, Y. W.; Go, G.; Lee, S. J.; Lee, G. H.; Kim, K. J.; Stiles, M. D.; Park, B. G.; Lee, K. J. Spin currents and spin–orbit torques in ferromagnetic trilayers. *Nat. Mater.* **2018**, *17*, 509.
- (14) You, L.; Lee, O.; Bhowmik, D.; Labanowski, D.; Hong, J.; Bokor, J.; Salahuddin, S. Switching of perpendicularly polarized nanomagnets with spin orbit torque without an external magnetic field by engineering a tilted anisotropy. *Proc. Natl. Acad. Sci. U. S. A.* **2015**, *112*, 10310.
- (15) Yu, G.; Upadhyaya, P.; Fan, Y.; Alzate, J. G.; Jiang, W.; Wong, K. L.; Takei, S.; Bender, S. A.; Chang, L.-T.; Jiang, Y.; Lang, M.; Tang, J.; Wang, Y.; Tserkovnyak, Y.; Amiri, P. K.; Wang, K. L. Switching of perpendicular magnetization by spin-orbit torques in the absence of external magnetic fields. *Nat. Nanotechnol.* **2014**, *9*, 548.
- (16) Cai, K.; Yang, M.; Ju, H.; Wang, S.; Ji, Y.; Li, B.; Edmonds, K. W.; Sheng, Y.; Zhang, B.; Zhang, N.; Liu, S.; Zheng, H.; Wang, K. Electric field control of deterministic current-induced magnetization switching in a hybrid ferromagnetic/ferroelectric structure. *Nat. Mater.* **2017**, *16*, 712.
- (17) Chen, S.; Yu, J.; Xie, Q.; Zhang, X.; Lin, W.; Liu, L.; Zhou, J.; Shu, X.; Guo, R.; Zhang, Z.; Chen, J. Free Field Electric Switching of Perpendicularly Magnetized Thin Film by Spin Current Gradient. *ACS Appl. Mater. Interfaces* **2019**, *11*, 30446.
- (18) Cao, Y.; Sheng, Y.; Edmonds, K. W.; Ji, Y.; Zheng, H.; Wang, K. Deterministic Magnetization Switching Using Lateral Spin-Orbit Torque. *Adv. Mater.* **2020**, *32*, 1907929.
- (19) Ma, Q.; Li, Y.; Gopman, D. B.; Kabanov, Y. P.; Shull, R. D.; Chien, C. L. Switching a Perpendicular Ferromagnetic Layer by Competing Spin Currents. *Phys. Rev. Lett.* **2018**, *120*, 117703.
- (20) Dzyaloshinsky, I. A. thermodynamic theory of “weak” ferromagnetism of antiferromagnetics. *J. Phys. Chem. Solids* **1958**, *4*, 241.
- (21) Moriya, T. Anisotropic Superexchange Interaction and Weak Ferromagnetism. *Phys. Rev.* **1960**, *120*, 91.
- (22) Fert, A.; Reyren, N.; Cros, V. Magnetic skyrmions: advances in physics and potential applications. *Nat. Rev. Mater.* **2017**, *2*, 17031.
- (23) Luo, Z.; Dao, T. P.; Hrabec, A.; Vijayakumar, J.; Kleibert, A.; Baumgartner, M.; Kirk, E.; Cui, J.; Savchenko, T.; Krishnaswamy, G.; Heyderman, L. J.; Gambardella, P. Chirally coupled nanomagnets. *Science* **2019**, *363*, 1435.
- (24) Han, D.-S.; Lee, K.; Hanke, J.-P.; Mokrousov, Y.; Kim, K.-W.; Yoo, W.; van Hees, Y. L. W.; Kim, T.-W.; Lavrijsen, R.; You, C.-Y.; Swagten, H. J. M.; Jung, M.-H.; Kläui, M. Long-range chiral exchange interaction in synthetic antiferromagnets. *Nat. Mater.* **2019**, *18*, 703.
- (25) Fernández-Pacheco, A.; Vedmedenko, E.; Ummelen, F.; Mansell, R.; Petit, D.; Cowburn, R. P. Symmetry-breaking interlayer Dzyaloshinskii–Moriya interactions in synthetic antiferromagnets. *Nat. Mater.* **2019**, *18*, 679.
- (26) Fert, A.; Levy, P. M. Role of Anisotropic Exchange Interactions in Determining the Properties of Spin-Glasses. *Phys. Rev. Lett.* **1980**, *44*, 1538.
- (27) Levy, P. M.; Fert, A. Anisotropy induced by nonmagnetic impurities in CuMn spin-glass alloys. *Phys. Rev. B: Condens. Matter Mater. Phys.* **1981**, *23*, 4667.
- (28) Yang, H.; Thiaville, A.; Rohart, S.; Fert, A.; Chshiev, M. Anatomy of Dzyaloshinskii–Moriya Interaction at Co/Pt Interfaces. *Phys. Rev. Lett.* **2015**, *115*, 267210.
- (29) Ma, X.; Yu, G.; Tang, C.; Li, X.; He, C.; Shi, J.; Wang, K. L.; Li, X. Interfacial Dzyaloshinskii–Moriya Interaction: Effect of 5d Band Filling and Correlation with Spin Mixing Conductance. *Phys. Rev. Lett.* **2018**, *120*, 157204.
- (30) Radu, I.; Vahaplar, K.; Stamm, C.; Kachel, T.; Pontius, N.; Dürr, H. A.; Ostler, T. A.; Barker, J.; Evans, R. F. L.; Chantrell, R. W.; Tsukamoto, A.; Itoh, A.; Kirilyuk, A.; Rasing, T.; Kimel, A. V. Transient ferromagnetic-like state mediating ultrafast reversal of antiferromagnetically coupled spins. *Nature* **2011**, *472*, 205.
- (31) Pizzini, S.; Vogel, J.; Rohart, S.; Buda-Prejbeanu, L. D.; Jué, E.; Boule, O.; Miron, I. M.; Saifeer, C. K.; Auffret, S.; Gaudin, G.; Thiaville, A. Chirality-Induced Asymmetric Magnetic Nucleation in

Pt/Co/AlO_x Ultrathin Microstructures. *Phys. Rev. Lett.* **2014**, *113*, 047203.

(32) Caretta, L.; Mann, M.; Büttner, F.; Ueda, K.; Pfau, B.; Günther, C. M.; Hessing, P.; Churikova, A.; Klose, C.; Schneider, M.; Engel, D.; Marcus, C.; Bono, D.; Bagschik, K.; Eisebitt, S.; Beach, G. S. D. Fast current-driven domain walls and small skyrmions in a compensated ferrimagnet. *Nat. Nanotechnol.* **2018**, *13*, 1154.

(33) Endo, M.; Kanai, S.; Ikeda, S.; Matsukura, F.; Ohno, H. Electric-field effects on thickness dependent magnetic anisotropy of sputtered MgO/Co₄₀Fe₄₀B₂₀/Ta structures. *Appl. Phys. Lett.* **2010**, *96*, 212503.

(34) Yang, H. X.; Chshiev, M.; Dieny, B.; Lee, J. H.; Manchon, A.; Shin, K. H. First-principles investigation of the very large perpendicular magnetic anisotropy at Fe/MgO and Co/MgO interfaces. *Phys. Rev. B: Condens. Matter Mater. Phys.* **2011**, *84*, 054401.

(35) Yu, G.; Chang, L. T.; Akyol, M.; Upadhyaya, P.; He, C. L.; Li, X.; Wong, K. L.; Amiri, P. K.; Wang, K. L. Current-driven perpendicular magnetization switching in Ta/CoFeB/[TaO_x or MgO/TaO_x] films with lateral structural asymmetry. *Appl. Phys. Lett.* **2014**, *105*, 102411.

(36) Ma, X.; Yu, G.; Li, X.; Wang, T.; Wu, D.; Olsson, K. S.; Chu, Z.; An, K.; Xiao, J. Q.; Wang, K. L.; Li, X. Interfacial control of Dzyaloshinskii–Moriya interaction in heavy metal/ferromagnetic metal thin film heterostructures. *Phys. Rev. B: Condens. Matter Mater. Phys.* **2016**, *94*, 180408.

(37) Kim, D.-H.; Haruta, M.; Ko, H.-W.; Go, G.; Park, H.-J.; Nishimura, T.; Kim, D.-Y.; Okuno, T.; Hirata, Y.; Futakawa, Y.; Yoshikawa, H.; Ham, W.; Kim, S.; Kurata, H.; Tsukamoto, A.; Shiota, Y.; Moriyama, T.; Choe, S.-B.; Lee, K.-J.; Ono, T. Bulk Dzyaloshinskii–Moriya interaction in amorphous ferrimagnetic alloys. *Nat. Mater.* **2019**, *18*, 685.

(38) Legrand, W.; Chauleau, J.-Y.; Maccariello, D.; Reyren, N.; Collin, S.; Bouzehouane, K.; Jaouen, N.; Cros, V.; Fert, A. Hybrid chiral domain walls and skyrmions in magnetic multilayers. *Sci. Adv.* **2018**, *4*, No. eaat0415.

(39) Li, W.; Bykova, I.; Zhang, S.; Yu, G.; Tomasello, R.; Carpentieri, M.; Liu, Y.; Guang, Y.; Gräfe, J.; Weigand, M.; Burn, D. M.; van der Laan, G.; Hesjedal, T.; Yan, Z.; Feng, J.; Wan, C.; Wei, J.; Wang, X.; Zhang, X.; Xu, H.; Guo, C.; Wei, H.; Finocchio, G.; Han, X.; Schütz, G. Anatomy of Skyrmionic Textures in Magnetic Multilayers. *Adv. Mater.* **2019**, *31*, 1807683.

(40) Parkin, S. S. P.; Kaiser, C.; Panchula, A.; Rice, P. M.; Hughes, B.; Samant, M.; Yang, S.-H. Giant tunnelling magnetoresistance at room temperature with MgO (100) tunnel barriers. *Nat. Mater.* **2004**, *3*, 862.

(41) Yuasa, S.; Nagahama, T.; Fukushima, A.; Suzuki, Y.; Ando, K. Giant room-temperature magnetoresistance in single-crystal Fe/MgO/Fe magnetic tunnel junctions. *Nat. Mater.* **2004**, *3*, 868.